ARTICLES

Bose-Einstein condensation of exciton polaritons

J. Kasprzak¹, M. Richard², S. Kundermann², A. Baas², P. Jeambrun², J. M. J. Keeling³, F. M. Marchetti⁴, M. H. Szymańska⁵, R. André¹, J. L. Staehli², V. Savona², P. B. Littlewood⁴, B. Deveaud² & Le Si Dang¹

Phase transitions to quantum condensed phases—such as Bose-Einstein condensation (BEC), superfluidity, and superconductivity—have long fascinated scientists, as they bring pure quantum effects to a macroscopic scale. BEC has, for example, famously been demonstrated in dilute atom gas of rubidium atoms at temperatures below 200 nanokelvin. Much effort has been devoted to finding a solid-state system in which BEC can take place. Promising candidate systems are semiconductor microcavities, in which photons are confined and strongly coupled to electronic excitations, leading to the creation of exciton polaritons. These bosonic quasi-particles are 10° times lighter than rubidium atoms, thus theoretically permitting BEC to occur at standard cryogenic temperatures. Here we detail a comprehensive set of experiments giving compelling evidence for BEC of polaritons. Above a critical density, we observe massive occupation of the ground state developing from a polariton gas at thermal equilibrium at 19 K, an increase of temporal coherence, and the build-up of long-range spatial coherence and linear polarization, all of which indicate the spontaneous onset of a macroscopic quantum phase.

Bosons—particles with an integer spin—can undergo BEC when their de Broglie wavelength becomes comparable to their average separation. Then a large fraction of the bosons condense in the lowest quantum state, resulting in the appearance of macroscopic coherence. Massive occupation of the ground state^{1,2} and the expected spontaneous coherence^{3–5} have been clearly demonstrated for dilute atom gases cooled down to temperatures of about 10^{–6} K.

For solid-state systems, excitons in semiconductors have long been considered a promising candidate for BEC at temperatures of a few kelvin, reachable by standard cryogenic techniques^{6–8}. Excitons are light-mass Bose particles analogous to positronium, consisting of bound electron–hole pairs, usually produced by optical excitation. Over the past three decades there have been numerous studies and early claims of exciton BEC in three-dimensional (3D) semiconductors (for a recent review see refs 9 and 10). Other systems in the solid state have also exhibited unusual physical properties tentatively attributed to BEC^{11,12}.

Recently new directions have been explored for exciton BEC, using two-dimensional (2D) quantum structures, such as coupled quantum wells under an external applied electric field 13,14 , or quantum wells embedded in optical microcavities. The second system consists in planar Fabry–Perot resonators whose optical length is tuned to a half-integer multiple of the emission wavelength of quantum well excitons. The near-degeneracy and strong coupling of the exciton and cavity photon leads to the formation of new eigenstates (see Fig. 1) called polaritons, which are half-light, half-matter bosonic quasiparticles 15,16 . The extremely steep dispersion of the cavity polariton modes, due to the optical confinement along the *z* direction, results in a typical polariton effective mass of 10^{-4} times the free electron mass. Thus, in theory, the temperature and density criteria for BEC of polaritons in their $k_{\parallel}=0$ ground state should be satisfied much more easily than for excitons. Moreover, from the experimental side,

we note that the coherence, polarization and population distribution properties of polaritons can be conveniently probed by analysing the far-field emission, because the light emitted by the microcavity is part of the polariton wavefunction 17 . The drawback of the strong coupling is the very short polariton lifetime, typically of around 10^{-12} s, which could be an obstacle to reach thermal equilibrium. Although full thermalization cannot be achieved with the host lattice, it will be shown below that polariton–polariton scattering processes are fast enough under high excitation to produce a fully thermalized polariton gas.

The first indication of spontaneous quantum degeneracy of polaritons was the observation of stimulated emission under non-resonant pumping in CdTe microcavities¹⁸: above some excitation power threshold, the polariton emission exhibits a strong nonlinearity, while the linewidth shows significant narrowing. Since then several claims of polariton condensation have been made. In particular, the second-order time correlations in a GaAs-based microcavity were measured to support such a claim¹⁹. However, no measurement of the polarization or of the spatial coherence is performed. Also, the second-order correlations do not follow the expected signature: at the stimulation threshold they are found to be quasi-thermal, and above threshold remain far from that expected for a coherent state. Of the defining features of BEC—that is, spontaneous symmetry breaking and long-range order^{20,21}—no direct proof in semiconductor systems has ever been given^{9,10}.

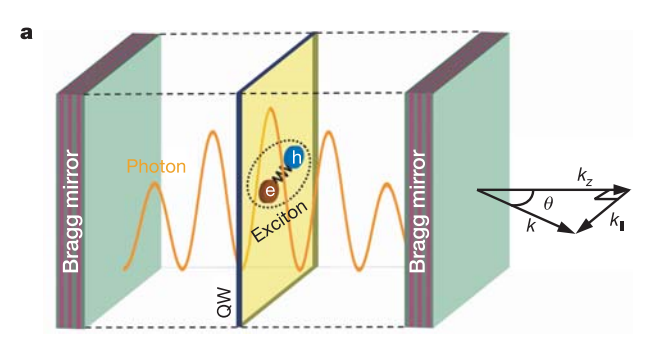
Of course, an infinite 2D system never develops true long-range order (see the Supplementary Information)²². However, owing to the finite size of the excitation spot, the size of the polariton cloud is finite, and one can achieve complete coherence across the cloud at low enough temperatures and macroscopic occupation of a single quantum state. Polaritons also have some specific features: first, they exhibit strong interactions even at modest densities^{23,24}, so the

¹CEA-CNRS-UJF joint group 'Nanophysique et Semiconducteurs', Laboratoire de Spectrométrie Physique (CNRS UMR5588), Université J. Fourier-Grenoble, F-38402 Saint Martin d'Hères cedex, France. ²Ecole Polytechnique Fédérale de Lausanne (EPFL), Station 3, CH-1015 Lausanne, Switzerland. ³MIT, Department of Physics, 77 Massachusetts Avenue, Cambridge, Massachusetts 02139-4307, USA. ⁴Cavendish Laboratory, Department of Physics, University of Cambridge, J. J. Thomson Avenue, Cambridge CB3 0HE, UK. ⁵Clarendon Laboratory, Department of Physics, University of Oxford, Parks Road, Oxford OX1 3PU, UK.

physics soon exits the regime of weakly interacting bosons that describes ultracold atoms; second, the lifetime is short enough that we must confront the role of non-equilibrium physics²⁵. Nevertheless, the principal experimental characteristics expected for BEC are clearly reported here: condensation into the ground state arising out of a population at thermal equilibrium; the development of quantum coherence, indicated by long-range spatial coherence, and sharpening of the temporal coherence of the emission.

Experimental procedure

The sample we studied consists of a CdTe/CdMgTe microcavity grown by molecular beam epitaxy. It contains 16 quantum wells,



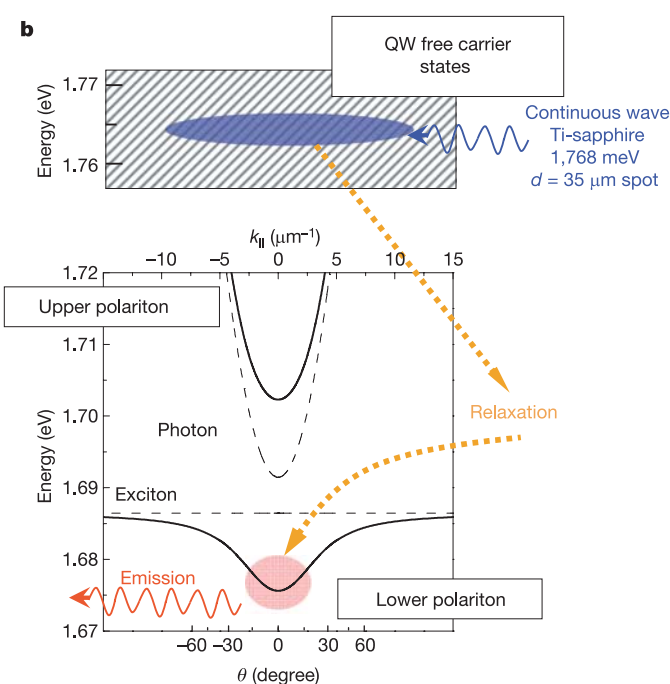


Figure 1 | Microcavity diagram and energy dispersion. a, A microcavity is a planar Fabry-Perot resonator with two Bragg mirrors at resonance with excitons in quantum wells (QW). The exciton is an optically active dipole that results from the Coulomb interaction between an electron in the conduction band and a hole in the valence band. In microcavities operating in the strong coupling regime of the light-matter interaction, 2D excitons and 2D optical modes give rise to new eigenmodes, called microcavity polaritons. **b**, Energy levels as a function of the in-plane wavevector k_{\parallel} in a CdTe-based microcavity. Interaction between exciton and photon modes, with parabolic dispersions (dashed curves), gives rise to lower and upper polariton branches (solid curves) with dispersions featuring an anticrossing typical of the strong coupling regime. The excitation laser is at high energy and excites free carrier states of the quantum well. Relaxation towards the exciton level and the bottom of the lower polariton branch occurs by acoustic and optical phonon interaction and polariton scattering. The radiative recombination of polaritons results in the emission of photons that can be used to probe their properties. Photons emitted at angle θ correspond to polaritons of energy E and in-plane wavevector $k_{\parallel} = (E/\hbar c)\sin\theta$.

displaying a vacuum field Rabi splitting of 26 meV (ref. 26). The microcavity was excited by a continuous-wave Ti:sapphire laser, combined with an acousto-optic modulator (1-µs pulse, 1% duty cycle) to reduce sample heating. The pulse duration is sufficiently long (by four orders of magnitude) in comparison with the characteristic times of the system to guarantee a steady-state regime. The laser beam was carefully shaped into a 'top hat' intensity profile providing a uniform excitation spot of about 35 µm in diameter on the sample surface, as shown in Fig. 4i. The excitation energy was 1.768 eV, well above the polariton ground state (1.671 eV at cavity exciton resonance), at the first reflectivity minimum of the Bragg mirrors, allowing proper coupling to the intra-cavity field. This ensures that polaritons initially injected in the system are incoherent, which is a necessary condition for demonstrating BEC. In atomic BEC or superfluid helium, the temperature is the parameter driving the phase transition. Here the excitation power, and thus the injected polariton density, is an easily tunable parameter, and so we chose it as the experimental control parameter. The large exciton binding energy in CdTe quantum wells (25 meV), combined with the large number of quantum wells in the microcavity, is crucial in maintaining the strong coupling regime of polaritons at high carrier density. The far-field polariton emission pattern was measured to probe the population distribution along the lower polariton branch. The spatially resolved emission and its coherence properties are accessible in a real-space imaging set-up combined with an actively stabilized

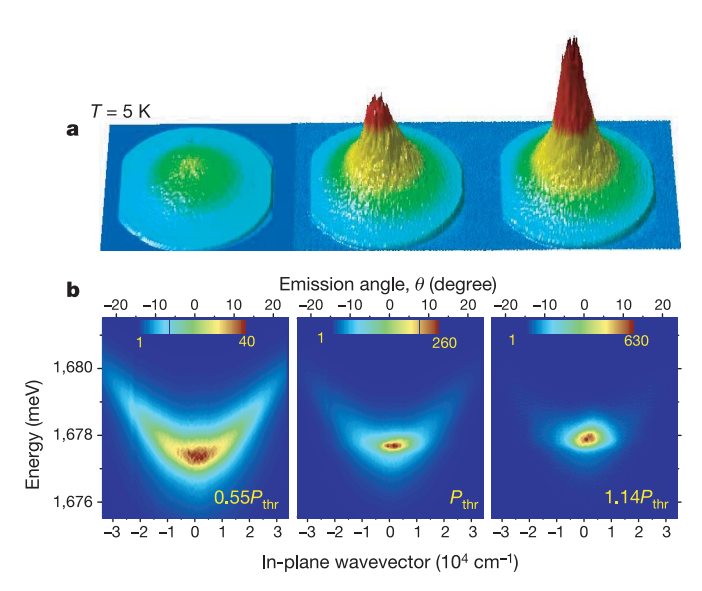


Figure 2 | Far-field emission measured at 5 K for three excitation intensities. Left panels, $0.55\,P_{\rm thr}$; centre panels, $P_{\rm thr}$; and right panels, $1.14 P_{\text{thr}}$; where $P_{\text{thr}} = 1.67 \text{ kW cm}^{-2}$ is the threshold power of condensation. a, Pseudo-3D images of the far-field emission within the angular cone of $\pm 23^{\circ}$, with the emission intensity displayed on the vertical axis (in arbitrary units). With increasing excitation power, a sharp and intense peak is formed in the centre of the emission distribution ($\theta_r = \theta_v = 0^\circ$), corresponding to the lowest momentum state $k_{\parallel} = 0$. **b**, Same data as in **a** but resolved in energy. For such a measurement, a slice of the far-field emission corresponding to $\theta_x = 0^\circ$ is dispersed by a spectrometer and imaged on a charge-coupled device (CCD) camera. The horizontal axes display the emission angle (top axis) and the in-plane momentum (bottom axis); the vertical axis displays the emission energy in a false-colour scale (different for each panel; the units for the colour scale are number of counts on the CCD camera, normalized to the integration time and optical density filters, divided by 1,000 so that 1 corresponds to the level of dark counts: 1,000). Below threshold (left panel), the emission is broadly distributed in momentum and energy. Above threshold, the emission comes almost exclusively from the $k_{\parallel}=0$ lowest energy state (right panel). A small blue shift of about 0.5 meV, or 2% of the Rabi splitting, is observed for the ground state, which indicates that the microcavity is still in the strong coupling regime.

Michelson interferometer to study phase spatial correlations. Experiments discussed in this work were performed for a slightly positive cavity—exciton detuning (3 to 8 meV).

Thermalization and condensation

Under non-resonant and high excitation, the polariton emission in CdTe-based microcavities becomes highly nonlinear^{18,27–30}. We first analyse the spectral and angular distribution of the emission as a function of the excitation power. Figure 2a displays pseudo-3D images of the angular distribution of the spectrally integrated emission. Below threshold (left), the emission exhibits a smooth distribution around $\theta_x = \theta_y = 0^\circ$, that is, around $k_{\parallel} = 0$. When the excitation intensity is increased, the emission from the zero momentum state becomes predominant at threshold (centre) and a sharp peak forms at $k_{\parallel} = 0$ above threshold (right). Figure 2b shows the energy and angle-resolved emission intensities. The width of the momentum distribution shrinks with increasing excitation intensity, and above threshold, the emission mainly comes from the lowest energy state at $k_{\parallel} = 0$. The polariton occupancy has been extracted from such emission patterns by taking into account the radiative lifetime of polaritons.

Figure 3a shows the occupancy of the ground state, as well as its emission energy and linewidth as a function of excitation power. With increasing excitation power, the occupancy first increases linearly, then exponentially, with sharp threshold-like behaviour. It should be noted that the occupancy at threshold is close to unity, consistent with a polariton relaxation process stimulated by the ground-state population: a specific feature of bosons. The emission blue shift was measured to be less than a tenth of the Rabi splitting at a pumping level ten times above the nonlinear threshold, confirming that the microcavity is still in the strong coupling regime. We measured the ordinary lasing excitation threshold and found it to be 50 times higher than the condensation threshold (not shown).

The linewidth of the $k_{\parallel} = 0$ emission shows significant narrowing

at the nonlinear threshold^{29,30}, down to half of the polariton linewidth in the linear regime (Fig. 3a). The line broadening observed at higher excitation is due to decoherence induced by polariton self-interaction³¹. We studied the coherence time more directly using a Michelson interferometer (not shown). This measurement gives a coherence time of 1.5 ps below the nonlinear threshold, and 6 ps above threshold, consistent with the spectral narrowing observed at threshold.

Signatures of polariton coherence in CdTe-based microcavities have been previously reported^{28,29}. Macroscopic coherence in the momentum plane was observed above the nonlinear threshold²⁸. However, the use of a small excitation spot (3 µm diameter) prevented relaxation into the lowest polariton energy states: polariton stimulation occurred in excited states and was thus only remotely connected with BEC. An experiment under conditions more favourable to BEC (25-µm-diameter spot), in which polaritons could condense into the lowest energy state, indirectly showed the build-up of macroscopic coherence in real space above threshold²⁹. However, that measurement was obtained under pulsed excitation (150-fs pulses), thus precluding steady state in the system and mixing high polariton densities at short times and low densities at long times on the same spectra.

Figure 3b displays the occupancy of polaritons as a function of their energy. The occupancy is computed by measuring the intensity of the signal, taking into account the polariton radiative recombination rate and the efficiency of the collection set-up. The uncertainty may be estimated to be roughly a factor of two. The estimation has been performed for different detunings and the threshold is always observed for occupancies of the order of one, in agreement with all previous measurements. For the sake of simplicity, we have arbitrarily adjusted the ground-state occupancy to be one at threshold. At very low excitation power, the polariton occupancy is not thermalized^{29,32,33}. Close to threshold, the occupancy can be fitted with a Maxwell–Boltzmann distribution, indicating a polariton gas in

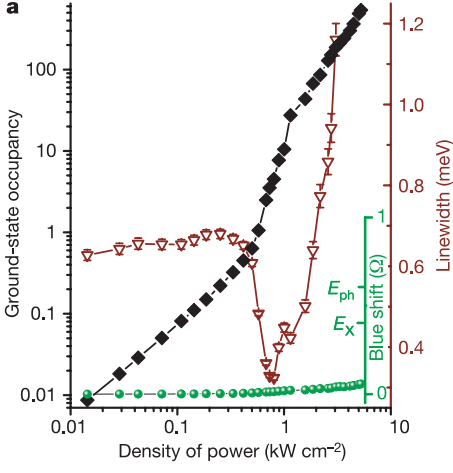
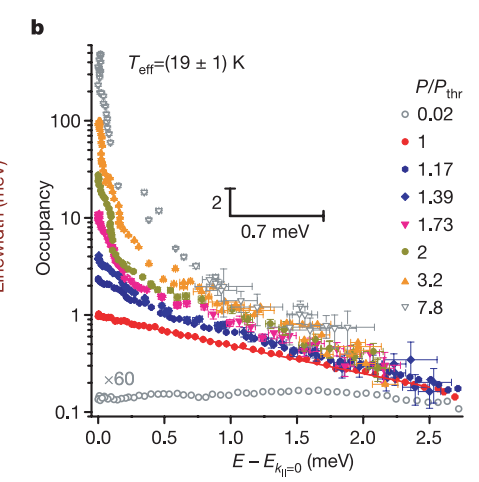


Figure 3 | Polariton occupancy measured at 5 K. a, Occupancy of the $k_{\parallel}=0$ ground state (solid black diamonds), its energy blue shift (solid green circles) and linewidth (open red triangles) versus the excitation power. The blue shift is plotted in units of the Rabi splitting $\Omega=26$ meV. At low excitation densities, the ground-state occupancy increases linearly with the excitation and then, immediately after threshold, increases exponentially before becoming linear again. This sharp transition is accompanied by a decrease of the linewidth by about a factor of two, corresponding to an increase of the polariton coherence. Further increase in linewidth is due to interaction between polaritons in the condensate. The polariton ground state slightly blue shifts, by less than 7% of the Rabi splitting for densities up to seven times the threshold density, staying well below the uncoupled exciton $(E_{\rm X})$ and photon mode $(E_{\rm ph})$ energies. This provides clear evidence of the strong coupling regime. b, Polariton occupancy in ground- and excited-state levels is plotted in a semi-logarithmic scale for various



excitation powers. For each excitation power, the zero of the energy scale corresponds to the energy of the $k_{\parallel}=0$ ground state. The occupancy is deduced from far-field emission data (see Fig. 2b), taking into account the radiative lifetime of polaritons. At the excitation threshold, the polariton gas is fully thermalized, as indicated by the Boltzmann-like exponential decay of the distribution function. Above threshold, the ground state becomes massively occupied, whereas the excited states are saturated, which is typical of BEC. The polariton thermal cloud is found to be at 19 K without significant changes when increasing the excitation to twice the threshold power. The low-energy part of the polariton occupancy cannot usually be properly fitted by a Bose distribution function, as expected for BEC of interacting particles. The error bars indicate standard deviation for each point; and the absolute uncertainty in occupation factor and polariton energy is given as the black scale bars.

thermal equilibrium at around 19 K. Above threshold, one can clearly observe a distribution featured by the saturation of the excited-state population and the formation of a condensate in the ground state. Saturation of excited levels and stability of the polariton temperature persist within a range $0.9 < P/P_{\text{thr}} < 2.3$ of excitation power. Such behaviour is typical of BEC, but, in general, we cannot obtain a reasonable fit for the low-energy part of the occupancy with a Bose-Einstein distribution. This is because in a non-ideal Bose system, interactions are responsible for changes in the density of states and depletion of the condensate in favour of excited states; such effects have been seen in atomic- and liquid-helium experiments^{34,35}. At first sight, the observation of an internal thermal equilibrium for polaritons could appear puzzling, considering the short polariton radiative lifetime. In fact, strong broadening of the polariton emission along the dispersion curve for excitation around threshold shows that the dephasing time due to polariton-polariton scattering is shorter than the polariton lifetime by a factor of two (not shown). Such a mechanism has been proposed for polariton BEC³⁶ and could indeed permit attainment of internal thermal equilibrium before the escape of polaritons out of the microcavity. Above threshold, the relaxation towards the condensed state should be enhanced thanks to stimulated scattering, whereas the polaritons are not expected to exhibit a reduced lifetime at high density. This fact should even favour the attainment of thermodynamical equilibrium in the condensed phase.

It is instructive to compare the density and temperature of thermalized polaritons (extracted from the occupancy of Fig. 3) with the theoretical predictions of the phase boundary^{23,24}. At $P=0.9\,P_{\rm thr}$ where thermalization but no condensation is observed, we estimate a density of around $5\times10^8\,{\rm cm}^{-2}$, which lies just above the theoretical threshold density for condensation at $T_{\rm eff}=19\,{\rm K}$ (see Supplementary Information).

Because BEC is a transition from an incoherent population to a

coherent matter wave, the most important property to be explored is the order parameter of the system, the macroscopic wavefunction of the condensate. As stated before, the condensed fraction should be described by a single wavefunction, and so we expect a clear polarization of the light, and a stationary phase across the whole condensate.

Linear polarization build-up

We measured the linear and circular polarization of the polariton emission, using either circularly or linearly polarized excitation. Below the nonlinear threshold, the emission appears to be completely depolarized (Fig. 4a–c). However, above threshold, a linear polarization of up to 83% spontaneously develops for $k_{\parallel}=0$ polaritons, whatever the polarization of the excitation (Fig. 4a, d, e)³⁷. The polarization direction is found to be approximately aligned along the [110] axis of the microcavity. For this striking result we consider possible explanations other than BEC.

First, any Bragg-based microcavity displays a longitudinal/transverse splitting due to the Fresnel laws. However, this splitting should vanish for vanishing incidence angle, that is for $k_{\parallel}=0$. Second, it could be argued that this polarization is inherited from the excitation through some parametric amplification process^{38,39}. Then, in this case, the polarization of the emission above the nonlinear threshold should be strongly dependent on the laser polarization. Such a correlation was not observed for either circularly or linearly polarized excitation (Fig. 4a), which rules out the hypothesis of parametric amplification.

We also checked the polarization of the emission spot. Below threshold the emission spot is homogeneous (Fig. 4h) and depolarized (not shown). Above threshold it becomes highly inhomogeneous, breaking into several ~4-µm spots which emit with the same linear polarization (see Fig. 4f and g). A careful examination of

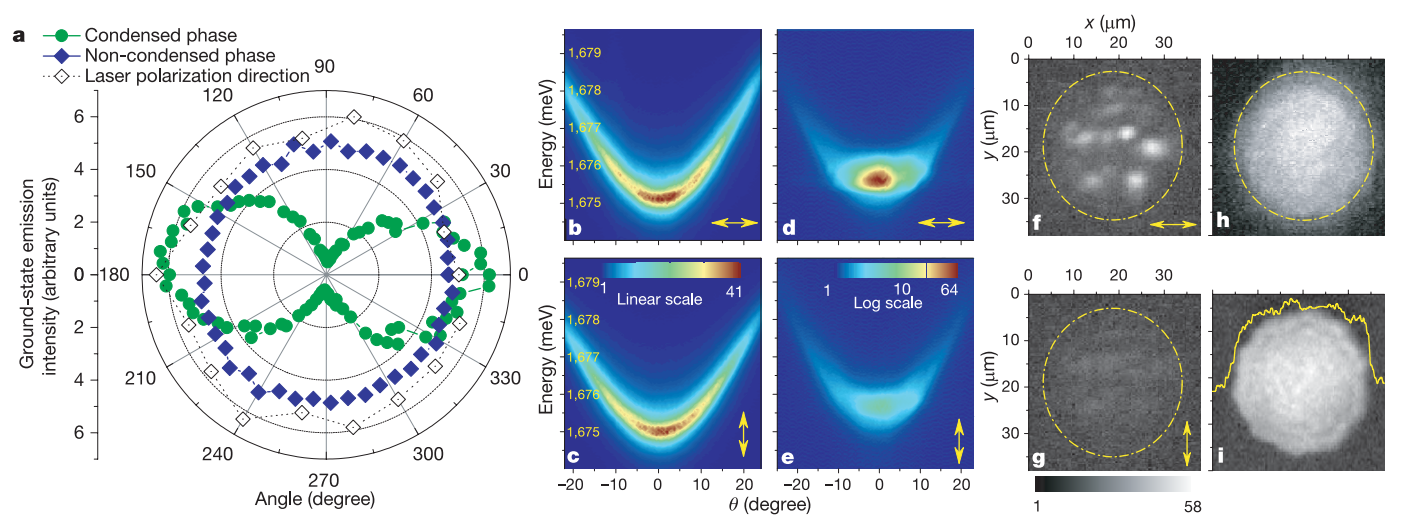


Figure 4 | **Polarization properties of the polariton emission. a**, The polar plot displays the intensity of the ground state emission at $k_{\parallel}=0$ (within a 0.4° aperture) measured as a function of the angle of the linear analyser. Below threshold (solid blue diamonds), the emission is completely depolarized for linear and circular (not shown) polarization, whereas above threshold (solid green circles) a linear polarization exceeding 80% is observed. The linear polarization is 'horizontal' (0, 180°), roughly aligned along the [110] crystalline axis. Open diamonds represent the intensity of the linearly polarized emission above threshold, measured as a function of the linear polarization angle of the excitation laser. No correlation can be found between the excitation polarization and the polariton polarization. -b-e, Analysis of the linear polarization (the doubleheaded yellow arrows indicate vertical or horizontal polarization of the detection) of the polariton emission below (b, c) and above (d, e) threshold. Below threshold, polaritons along the dispersion curve are not polarized because their

emission intensity is the same for horizontal and vertical polarizations. Above threshold, emission from the excited states remains depolarized, but emission from the ground state is strongly linearly polarized. Note the linear and logarithmic scales (number of counts on the CCD divided by 1,000) used for the emission intensity measured below and above threshold, respectively. **b**, **d** and **e** have the same axes as **c**. **f**-i, Analysis of the linear polarization of the emitting spot below (**h**) and above (**f**, **g**) threshold. i shows the image of the excitation laser with its 'top hat' intensity profile. The greyscale applies to **f** and **g** (number of counts on the CCD camera divided by 1,000). **h** shows the emitting spot below threshold which appears homogeneous and depolarized (not shown). Above threshold, the emitting spot becomes inhomogeneous: several bright small spots, due to structural inhomogeneities, are observed within the excitation area. Each of them emits with the same linear polarization, consistent with the development of a single condensate. **h** and **i** have the same axes as **f** and **g**.

the emission below threshold reveals a splitting of the order of 0.1 meV between two linearly cross-polarized emissions at $k_{\parallel}=0$, most probably due to anisotropic photonic structural disorder. This splitting is much smaller than $kT\approx 1.6$ meV, and yet above threshold, the system selects the lowest energy of these two states⁴⁰. Such a selection, as observed in atomic BEC, is a strong indication that a phase transition has occurred.

The final step of our demonstration is the evidence of macroscopic phase coherence^{20,21}, that is, the direct measurement of long-range spatial correlations. In particular, it will rule out the possibility of several independent condensates.

Long-range spatial coherence

Spatial coherence has been investigated by measuring the classical first-order correlation function of the polariton emission:

$$g^{(1)}(\mathbf{r}, \mathbf{r}') = \frac{\langle E^*(\mathbf{r})E(\mathbf{r}')\rangle}{\langle E^*(\mathbf{r})\rangle\langle E(\mathbf{r}')\rangle}$$

where $E(\mathbf{r})$ is the electric field at point \mathbf{r} . For classical fields, $g^{(1)}(\mathbf{r}, \mathbf{r}')$ gives the amount of phase correlations between the fields at points \mathbf{r} and \mathbf{r}' without relative time delay. In the low-density regime, the polaritons are expected to exhibit short-range correlations, with a correlation length given by the thermal de Broglie wavelength. In the condensed phase, complete coherence, up to the size of the condensate is expected^{20,21}.

We combined a Michelson interferometer with a high-resolution

imaging set-up: two images of the condensate magnified 40 times, each coming from one arm of the interferometer, are combined at the output of the interferometer and overlap in the image plane, forming an interference pattern. One image can be displaced with respect to the other by any vector \mathbf{d} simply by tilting a mirror of the interferometer. The contrast C of the interference is measured for each point of the image plane by scanning the relative phase of the interferometer over $\sim 6\pi$, providing a direct measurement of the correlation function:

$$C(\mathbf{r}, \mathbf{d}) = \frac{I_{\text{max}} - I_{\text{min}}}{I_{\text{max}} + I_{\text{min}}} = \frac{2\sqrt{I(\mathbf{r})I(\mathbf{r} + \mathbf{d})}}{I(\mathbf{r}) + I(\mathbf{r} + \mathbf{d})}g^{(1)}(\mathbf{r}, \mathbf{r} + \mathbf{d})$$

in which I denotes light intensity and $I_{\rm max}$ and $I_{\rm min}$ denote the maximum and the minimum of the interference pattern (intensity versus phase). We first measured the first-order correlation between two small regions ($\sim\!4\,\mu{\rm m}^2$) of the emission separated by 6 $\mu{\rm m}$ (see Fig. 5a, b), as a function of the driving parameter—the excitation power. Below threshold, the interference contrast is below 5% resolution limited. Above the stimulation threshold, the contrast grows up to 45%, indicating a significant increase in the correlation length. Similar results have been obtained for any pair of bright spots chosen within the condensate.

Next, we measured the correlations between any pair of points \mathbf{r} and \mathbf{r}' symmetric with respect to the centre of the condensate. To do so, we replaced the mirror in one arm of the interferometer by a retro-reflector to invert the image in a centro-symmetric way. Thus,

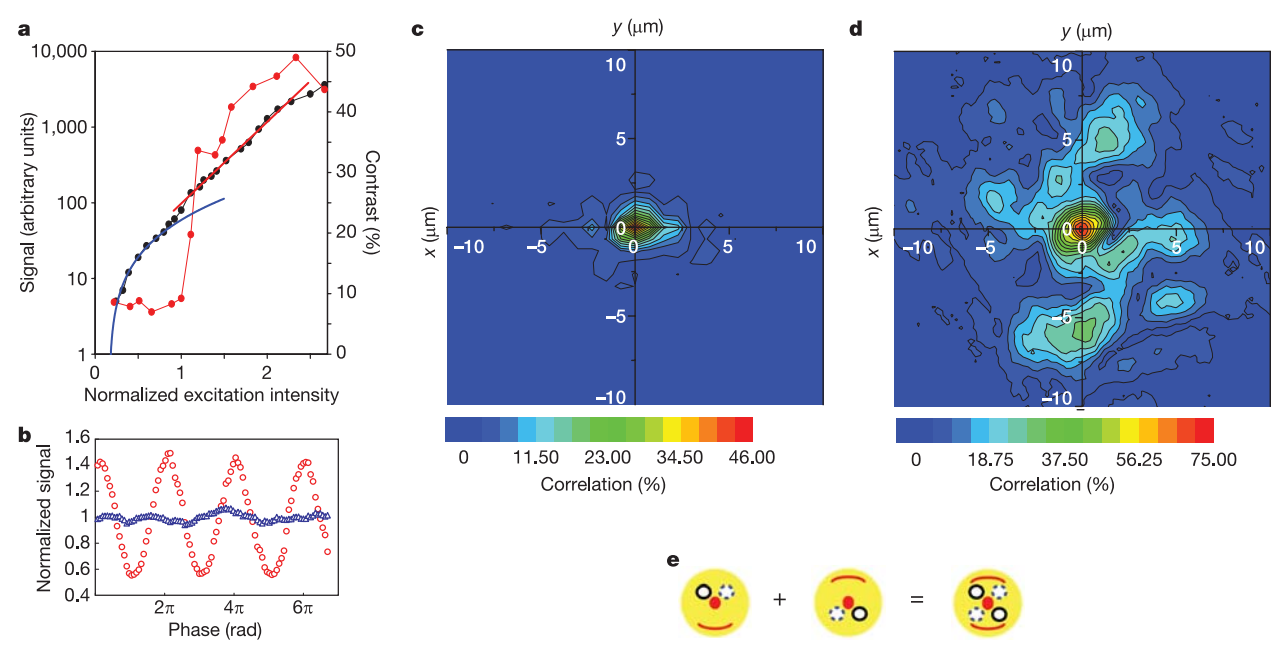


Figure 5 | Spatial correlation measurements using a Michelson interferometer. 3 Solid red circles indicate correlations between

interferometer. a, Solid red circles indicate correlations between two spots separated by 6 µm (2.5 times the thermal de Broglie wavelength) within the condensate as a function of the excitation power (the threshold power was $P_{\rm thr} = 4.5 \, {\rm kW \, cm^{-2}}$). The correlation exhibits a threshold-like behaviour: it starts to build up from a noise-limited value of 5-8% to 46% at excitation power twice the threshold power. The variation of the ground-state emission intensity, normalized to the excitation power, is shown for comparison (solid black circles). The solid blue line is a quadratic fit of the data demonstrating the occurrence of particle-particle interaction below threshold. Above threshold, the solid red line is an exponential fit demonstrating the strong stimulation of the relaxation by the high occupancy factor of the ground state. **b**, Typical interference fringes between spots 1 and 2 as a function of the relative phase (horizontal axis), measured below (open blue triangles) and above (open red circles) the nonlinear threshold, with contrasts of 5% and 46%, respectively. c, Correlation mapping below threshold using a linear colour scale. Each point (x, y) in the

map represents the correlation between points (x, y) and (-x, -y) of the condensate (see e for details). The correlation peak extends over 2.6 µm (full-width at half-maximum), thus providing a measurement of the de Broglie wavelength. d, Same as c but for excitation above threshold. Some islands with a high degree of correlation (up to 30%) are formed for distances as long as 4.5 times the thermal de Broglie wavelength. These islands correspond to the bright spots caused by the in-plane spatial disorder experienced by the condensate (see Fig. 4f). e, Schematic description of the experiment realized for correlation mapping in c and d. The first 'smiley' symbolizes the image originating from the first arm of the Michelson interferometer. The second arm produces an identical but flipped image with respect to a chosen point (here, the red nose). The resulting interference pattern consists in the overlap of the two images, each point corresponding to the interference between one point of the 'smiley' and its symmetric with respect to the nose. All experiments were done using a 20-µm-diameter spot with a gaussian intensity profile.

the contrast of the interference pattern gives $g^{(1)}(\mathbf{r}, -\mathbf{r})$. This configuration simultaneously provides the correlation between pairs of points separated by the quantity $\mathbf{d} = -2\mathbf{r}$ (Fig. 5e).

Correlations measured for $P=1.9\,P_{\rm thr}$ are displayed in Fig. 5d. Apart from the high correlation peak at the centre, which corresponds to the short-range correlations, several large islands with correlations exceeding 30% are observed for pairs of points separated by $|\mathbf{d}|=12\,\mu\mathrm{m}$. The range of these correlations is limited only by the finite size of the condensate. The variety of the island shapes reflects only the spatial inhomogeneity inherited from the in-plane disorder of the microcavity.

Below the nonlinear threshold, we find that the correlations vanish for distances as small as 2.6 μm . This coherence length corresponds to the thermal de Broglie wavelength of a homogenous thermalized polariton gas (see Fig. 3b and Fig. 4h). The condensate cloud is several times larger than this length (16 μm versus 2.6 μm), yet shows a correlations length of the order of its diameter, providing direct evidence of coherence across the entire condensate.

In conclusion, we have realized the condensation of exciton polaritons in a CdTe-based microcavity. Strictly speaking, the reported condensation is not a standard BEC because polaritons are not ideal (non-interacting) bosons, and are not in thermal equilibrium with the phonon bath. Moreover the polariton system is not conservative, in the sense that polaritons continuously leak out of the microcavity. Nevertheless all specific ingredients of a true BEC have been observed: above some critical density, condensation takes place in the ground state, out of a degenerate Bose gas fully thermalized at 19 K. The phase-transition character of the phenomenon is clearly seen, to our knowledge for the first time in the solid state, by the build-up of spatial coherence and macroscopic polarization across the entire condensate. These findings are promising for the development of the so-called 'polariton laser' 16,41 and Bose condensation at increased temperatures with wider bandgap semiconductors such as ZnO or GaN.

Received 18 April; accepted 24 July 2006.

- Anderson, M. N. et al. Observation of Bose-Einstein condensation in a dilute atomic vapor. Science 269, 198–201 (1995).
- Davis, K. B. et al. Bose-Einstein condensation in a gas of sodium atoms. Phys. Rev. Lett. 75, 3969–3973 (1995).
- Andrews, M. R. et al. Observation of interference between two Bose condensates. Science 275, 637–641 (1997).
- Burt, E. A. et al. Coherence, correlations, and collisions: What one learns about Bose-Einstein condensates from their decay. Phys. Rev. Lett. 79, 337–340 (1997).
- Bloch, I. et al. Measurement of the spatial coherence of a trapped Bose gas at the phase transition. Nature 403, 166–170 (2000).
- Moskalenko, S. A. Reversible optico-hydrodynamic phenomena in a non ideal exciton gas. Sov. Phys. Solid State 4, 199–204 (1962).
- Blatt, J. M. Bose-Einstein condensation of excitons. Phys. Rev. 126, 1691–1692 (1962).
- 8. Keldysh, L. V. & Kozlov, A. N. Collective properties of excitons in semiconductors. Sov. Phys. JETP 27, 521–525 (1968).
- Snoke, D. W. Spontaneous Bose coherence of excitons and polaritons. Science 298, 1368–1372 (2002).
- Snoke, D. W. When should we say we have observed Bose condensation of excitons? Phys. Status Solidi B 238, 389–396 (2003).
- Rüegg, Ch. et al. Bose-Einstein condensation of the triplet states in the magnetic insulator TICuCl₃. Nature 423, 62–65 (2003).
- Eisenstein, J. P. & MacDonald, A. H. Bose-Einstein condensation of excitons in bilayer electron systems. *Nature* 432, 691–694 (2004).
- 13. Butov, L. V. *et al.* Towards Bose-Einstein condensation of excitons in potential traps. *Nature* 417, 47–52 (2002).
- 14. Snoke, D. W. et al. Long-range transport in excitonic dark states in coupled quantum wells. *Nature* 418, 754–757 (2002).
- Weisbuch, C. et al. Observation of the coupled exciton-photon mode splitting in a semiconductor quantum microcavity. Phys. Rev. Lett. 69, 3314–3317 (1992).

- 16. Kavokin, A. & Malpuech, G. Cavity Polaritons (Elsevier, Amsterdam, 2003).
- Savona, V. et al. Theory of polariton photoluminescence in arbitrary semiconductor microcavity structures. Phys. Rev. B 53, 13051–13062 (1996).
- Le Si, D. et al. Stimulation of polariton photoluminescence in semiconductor microcavity. Phys. Rev. Lett. 81, 3920–3923 (1998).
- Deng, H. et al. Condensation of semiconductor microcavity exciton polaritons. Science 298, 199–202 (2002).
- Leggett, A. J. Bose-Einstein condensation in the alkali gases: Some fundamental concepts. Rev. Mod. Phys. 73, 307–356 (2001).
- Pitaevskii, L. & Stringari, S. Bose-Einstein Condensation Ch. 1, 6, 15 (Oxford Science Publication, Oxford Univ. Press, Oxford, 2003).
- Mermin, N. D. & Wagner, H. Absence of ferromagnetism or antiferromagnetism in one- or two-dimensional isotropic Heisenberg models. *Phys. Rev. Lett.* 17, 1133–1136 (1966).
- 23. Keeling, J. et al. Polariton condensation with localized excitons and propagating photons. *Phys. Rev. Lett.* **93**, 226403 (2004).
- Marchetti, F. M. et al. Thermodynamics and excitations of condensed polaritons in disordered microcavities. Phys. Rev. Lett. 96, 066405 (2006).
- Szymańska, M. H. et al. Non-equilibrium quantum condensation in an incoherently pumped dissipative system. Phys. Rev. Lett. 96, 230602 (2006).
- André, R. et al. Spectroscopy of polaritons in CdTe-based microcavities. J. Cryst. Growth 184/185, 758–762 (1998).
- Bœuf, F. et al. Evidence of polariton stimulation in semiconductor microcavities. Phys. Rev. B 62, R2279–R2282 (2000).
- Richard, M. et al. Spontaneous coherent phase transition of polaritons in CdTe microcavities. Phys. Rev. Lett. 94, 187401 (2005).
- Richard, M. et al. Experimental evidence for nonequilibrium Bose condensation of exciton polaritons. Phys. Rev. B 72, 201301(R) (2005).
- Bloch, J. et al. Monitoring the dynamics of a coherent cavity polariton population. Phys. Rev. B 71, 155311 (2005).
- 31. Porras, D. & Tejedor, C. Linewidth of a polariton laser: Theoretical analysis of self-interaction effects. *Phys. Rev. B* **67**, 161310(R) (2003).
- Tassone, F. et al. Bottleneck effects in the relaxation and photoluminescence of microcavity polaritons. Phys. Rev. B 56, 7554–7563 (1997).
- Müller, M. et al. Dynamics of the cavity polariton in CdTe-based semiconductor microcavities: Evidence for a relaxation edge. Phys. Rev. B 62, 16886–16892 (2000).
- Ensher, J. R. et al. Bose-Einstein condensation in a dilute gas: Measurement of energy and ground state occupation. Phys. Rev. Lett. 77, 4984–4987 (1996).
- Sokol, P. in Bose-Einstein Condensation (eds Griffin, A., Snoke, D. W. & Stringari, S.) 51 (Cambridge Univ. Press, Cambridge, 1995).
- 36. Porras, D. et al. Polariton dynamics and Bose-Einstein condensation in semiconductor microcavities. *Phys. Rev. B* **66**, 85304 (2002).
- 37. Martin, M. D. et al. Striking dynamics of II-VI microcavity polaritons after linearly polarized excitation. *Phys. Status Solidi C* **2**, 3880–3883 (2005).
- Savvidis, P. G. et al. Angle-resonant stimulated polariton amplifier. Phys. Rev. Lett. 84, 1547–1550 (2000).
- Ciuti, C. et al. Parametric luminescence of microcavity polaritons. Phys. Rev. B 63, 041303(R) (2001).
- Laussy, F. P. et al. Effects of Bose-Einstein condensation of exciton polaritons in microcavities on the polarization of emitted light. *Phys. Rev. B* 73, 035315 (2006).
- Imamoglu, A. & Ram, R. J. Quantum dynamics of exciton lasers. Phys. Lett. A 214, 193–198 (1996).

Supplementary Information is linked to the online version of the paper at www.nature.com/nature.

Acknowledgements This work is dedicated to R. Romestain. We acknowledge support by the European Union Network "Photon-mediated phenomena in semiconductor nanostructures" and from the Swiss National Research Foundation through the "Quantum Photonics NCCR". We thank J.-P. Poizat, D. Sarchi and O. El Daïf for many discussions.

Author Contributions J.K., M.R., S.K. and A.B. contributed equally to this work: J.K. worked on 'Thermalization and condensation' and 'Linear polarization build-up'; M.R., S.K. and A.B. worked on the 'Long-range spatial coherence'. J.M.J.K., F.M.M. and M.H.S. performed theoretical modelling of the data and prepared the Supplementary Information.

Author Information Reprints and permissions information is available at www.nature.com/reprints. The authors declare no competing financial interests. Correspondence and requests for materials should be addressed to B.D. (benoit.deveaud-pledran@epfl.ch) and J.K. (jkasprz@spectro.ujf-grenoble.fr).